ACS OMEGA

http://pubs.acs.org/journal/acsodf

Article

Corrosion Inhibition of Carbon Steel in Hydrochloric Acid Solution Using Ethoxylated Nonionic Surfactants Based on Schiff Base: Electrochemical and Computational Investigations

Ahmed G. Bedir, Mohamed Abd El-raouf,* Samah Abdel-Mawgoud, Nabel A. Negm, and N. M. El Basiony*

Cite This: *ACS Omega* 2021, 6, 4300−4312

Read Online

ACCESS | Metrics & More | Article Recommendations

ABSTRACT: Two ethoxylated nonionic surfactants (L400 and L600) based on Schiff base are prepared from polyoxyethylene, glyoxalic acid, and phenylenediamine. They are evaluated electrochemically as carbon steel corrosion inhibitors in 1 M HCl by electrochemical impedance spectroscopy (EIS) and Tafel techniques and complemented with microscopic analysis methods. The obtained Tafel data indicate the mixed-type behavior of the inhibitor used. The inhibition efficiency touches the peak at 1×10^{-4} M, exhibiting 92 and 94% for L400 and L600, respectively. The presence of the tested inhibitors decreases corrosion current density (i_{corr}) and double-layer capacitance (C_{dl}) due to the formation of a protective adsorption layer in place of the already adsorbed water and aggressive Cl^- ions. Both L400 and L600 adsorption modes follow Langmuir adsorption isotherm. The density functional theory (DFT) calculated indices (ΔE_{gap} and E_{HOMO}) indicate the superiority of L600 over the L400 counterpart as a reactive compound. Adsorption of L600 and L400 over the Fe(1 1 0) in simulated acidic medium is investigated by Monte Carlo (MC) simulation to verify their inhibition performance and are matched with adsorption free energy ΔG_{ads} calculated values. Both experimental and theoretical data are in agreement.

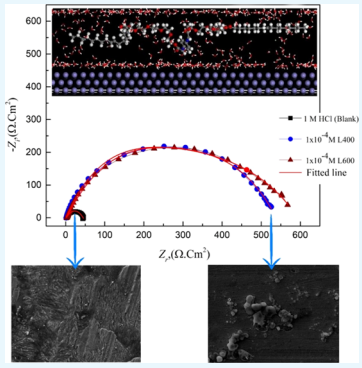

1. INTRODUCTION

Carbon steel is frequently used in innumerable engineering and manufacturing applications, including design and construction, as it has some excellent mechanical−chemical properties. However, one of the major dilemmas of using carbon steel is its susceptibility to corrosion.[1−3] Corrosion of carbon steel is an unavoidable but controllable process. Inhibitors are considered one of the essential additives tools to protect carbon steel corrosion. The acid pickling process is a common industrial cleaning process in petrochemical production and oil-well practices to remove mineral oxides and mineral scale depositions. Still, this process must be controllable due to the highly destructive corrosion effect of mineral acid used (HCl).[4] Eco-friendly organic inhibitor applications have emerged to meet the environmental demands. Therefore, inorganic inhibitors (such as chromates, molybdates, phosphates, and nitrates) are extensively used in the corrosion protection of metal/alloys (e.g., X65 carbon steel), which are replaced despite their high efficiency.[5−8] Organic surfactants, besides their eco-friendly and biodegradable features, also have corrosion inhibition feature. They have high electron density centers (N, P, and π electrons), which allows their adsorption over the metallic surface and shields the metal surface from the corrosive media.[9−11] We can find that recent trends of publications of environmental and eco-friendly corrosion inhibitors, according to the Sci-Finder database, are estimated to be 50% of the total publications of the corrosion inhibitors. Therefore, many researchers have focused on using environmental and eco-friendly inhibitors. Also, many researchers have focused on using nonionic inhibitors; for example, Al-Abdali et al. studied nonionic surfactants containing six-membered rings as oxazine;[12] Fouda et al. studied HENPEM surfethoxymer;[13] Shaban et al. studied nonionic dithiol surfactants (SH600);[14] Al-Sabagh et al. studied nonionic surfactants based on amino acid (S1);[15] and Abdallah et al. studied 4-(3,6,9,12-tetraoxatetracosyloxy) phenol,[16] which achieved an inhibition efficiency in the range from 31 up to 91%. The recently studied compounds achieved a good antimicrobial activity as evaluated elsewhere; also, the compounds are enriched with high electron density centers, which results in their high-potential applications as eco-friendly corrosion inhibitors with high efficiency, which reached 94%. In this work, we focused on the previously synthesized

Received: November 9, 2020
Accepted: January 20, 2021
Published: January 29, 2021

https://dx.doi.org/10.1021/acsomega.0c05476
ACS Omega 2021, 6, 4300−4312

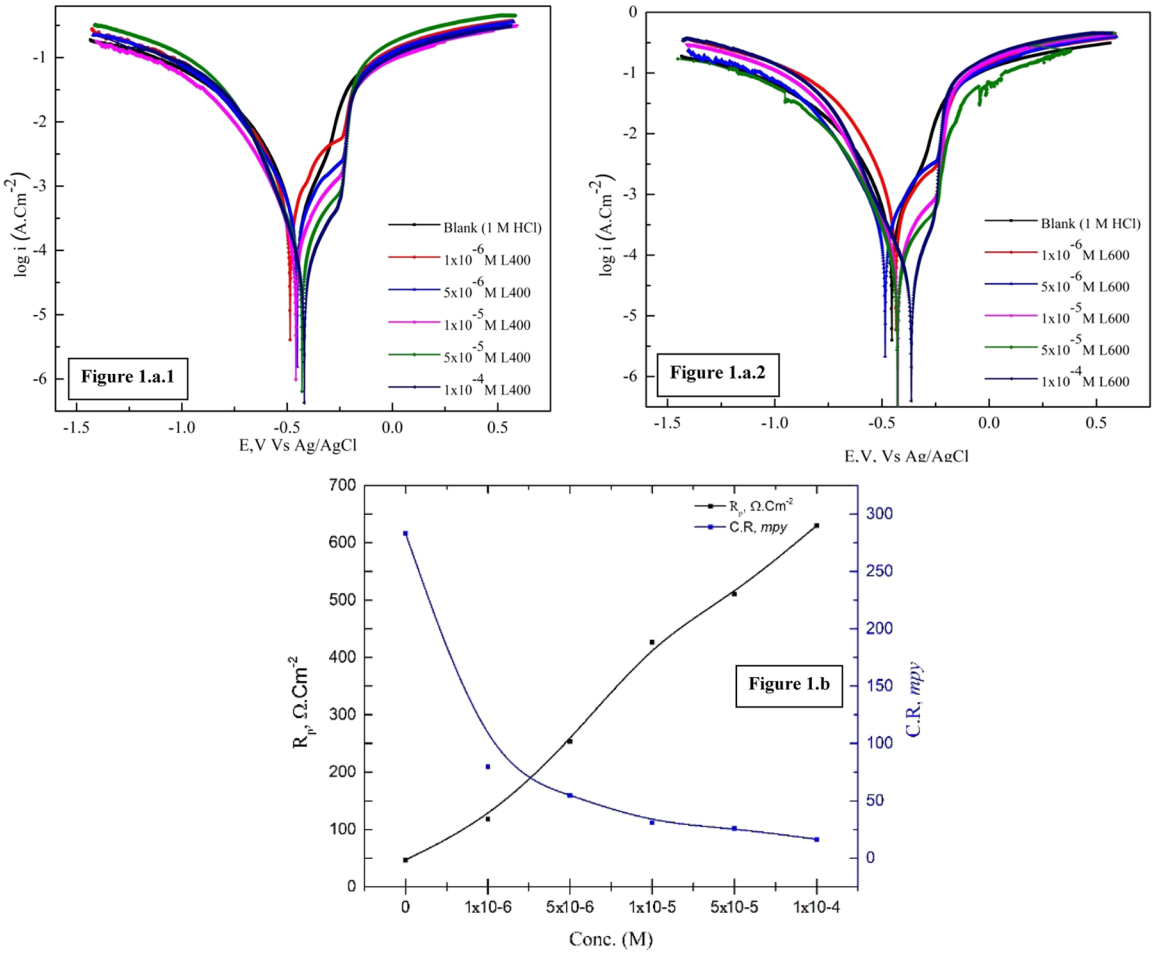

Figure 1. (a1) Polarization curves of the X65 steel in 1 M HCl in the absence and presence of different concentrations of the L400 inhibitor. (a2) Polarization curves of the X65 steel in 1 M HCl in the absence and presence of different concentrations of the L600 inhibitor. (b) Relation between C.R., R_p, and inhibitor concentrations.

nonionic surfactants (L400 and L600) as acid corrosion inhibitors for X65 carbon steel, which acts as a surface-active agent with good surface activity as well as a multifunctional compound. The chemical composition of the prepared molecules is mainly formed from poly(ethylene glycol) (PEG) and oleic acid, which have an eco-friendly behavior.[17] These characteristics give them the potentiality to act as novel corrosion inhibitors. The study included electrochemical tests such as electrochemical impedance spectroscopy (EIS) and potentiodynamic polarization (Tafel), complemented with surface morphology study (scanning electron microscopy (SEM) and energy-dispersive X-ray analysis (EDX)). The computational studies via density functional theory (DFT) and Monte Carlo simulations (MC) on the (1 1 0) Fe crystal were performed to confirm and support the experimental data.[18−20]

2. EXPERIMENTAL SECTION

2.1. Corrosion Test. *2.1.1. Solution.* Diluted 1 M HCl from 37% HCl is the tested aggressive media. The tested inhibitors' concentrations are in the range 1×10^{-6} to 1×10^{-4} M and are freshly prepared using bidistilled water.[21]

2.1.2. Metal Alloy X65 Steel. Elemental analysis of X65 used as a working electrode in wt % was 0.103 C; 0.210 Si; 0.024 P; 1.05 Mn; 0.012 Ni; 0.032 Co; and Fe balance.

2.2. Electrochemical Measurements. Auto-lab (PGSTAT128N) potentiostat/galvanostat with NOVA 2.1.4 software was used to perform the electrochemical corrosion tests at room temperature. The three-electrode system in a jacketed glass cell consisted of X65, Ag/AgCl (3 M KCl), and Pt as the working, reference, and auxiliary electrodes, respectively. The working electrode was mounted with the epoxy resin where the surface area exposed to the tested aggressive media was 0.283 cm^2. The exposed area was polished with different grades of SiC papers until 2500 to obtain a mirror image surface before each run. The electrochemical tests were conducted after 30 min of immersion in a tested solution.[22] The EIS measurements were conducted within the frequency range of 100 kHz to 0.1 Hz under potentiostatic conditions at an open-circuit potential (OCP) and an amplitude of 10 mV. The potentiodynamic polarization responses were sought without and with the addition of various concentrations of corrosion inhibitors (1×10^{-6}, 5×10^{-6}, 1×10^{-5}, 5×10^{-5}, and 1×10^{-4} M) for the tested (L400 and L600) compounds in 1 M HCl solution at 25 °C, while adopting a scan rate of 1 mV/s. Potentiodynamic sweeps were ±1 V vs OCP.[23] The inhibition efficiency (IE) and the surface coverage degree (θ) for EIS and Tafel data were calculated using eqs 1−4[24]

$$\theta = 1 - \left(\frac{R_{ct(o)}}{R_{ct(i)}} \right) \quad (1)$$

https://dx.doi.org/10.1021/acsomega.0c05476
ACS Omega 2021, 6, 4300−4312

Table 1. Potentiodynamic Polarization Measurements of the X65 Steel in 1 M HCl in the Absence and Presence of Various Concentrations of the L400 and L600 Nonionic Surfactants at 25 °C

	conc (M)	$-E_{corr}$vs Ag/AgCl (3 M KCl) (mV)	i_{corr} (μA/cm2)	$-\beta_c$ (mV/dec)	β_a (mV/dec)	R_p (Ω·cm^2)	CR (Mpy)	θ	IE (%)
blank		451	618	147.22	121.9	46.85	283.23		
L400	1×10^{-6}	434	186	95.84	52.366	79.05	85.24	0.6993	69.93
	5×10^{-6}	482	158	159.15	88.01	155.74	72.41	0.7436	74.36
	1×10^{-5}	430	89.8	175.67	106.98	321.50	41.15	0.8547	85.47
	5×10^{-5}	433	76.4	172.78	118.36	399.22	35.01	0.8763	87.63
	1×10^{-4}	423	48	157.27	104.85	569.09	21.99	0.9223	92.23
L600	1×10^{-6}	462	174	143.7	70.505	118.03	79.74	0.7181	71.81
	5×10^{-6}	463	119	182.73	111.84	253.15	54.53	0.8079	80.79
	1×10^{-5}	414	67.3	156.86	114.29	426.58	30.84	0.8911	89.11
	5×10^{-5}	397	56.7	142.64	125.16	510.53	25.98	0.9082	90.82
	1×0^{-4}	352	36	87.119	130.52	630.17	16.48	0.9418	94.18

$$\text{IE}\ (\%) = 1 - \left(\frac{R_{ct(o)}}{R_{ct(i)}}\right) \times 100 \quad (2)$$

$$\text{IE} = \left[1 - \left(\frac{I_{corr(i)}}{I_{corr(o)}}\right)\right] \times 100 \quad (3)$$

$$\theta = \left[1 - \left(\frac{I_{corr(i)}}{I_{corr(o)}}\right)\right] \quad (4)$$

where $R_{ct(o)}$ and $R_{ct(i)}$ are the charge-transfer resistances of C-steel in the absence and presence of inhibitors, respectively. $i_{corr(o)}$ and $i_{corr(i)}$ are the corrosion current densities of the steel specimen (A·cm^{-2}) in the absence and presence of different concentrations of the tested compounds (L400 and L600), respectively. Each electrochemical test was duplicated twice and the mean value was taken.

2.3. Surface Analysis Study. The aggressive action of HCl on the X65 surface was imaged in the absence and presence of 1 × 10^{-4} M of L600 after 3 h of treatment using SEM and EDX with the help of QUANTA FEG-250 at CMRDI.[25]

2.4. Quantum Calculation Method. Recently, theoretical calculations are necessary to simulate the experimental data. Quantum chemical calculations were done using Material Studio (MS 6.0; Accelrys) software in a vacuum and solvated phases. To study the chemical reactivity of L400 and L600 compounds, we apply the DMOL^3 module based on the gradient-corrected functional (GGA) method with Becke One Parameter (BOP) and double numerical polarized (DNP) basis set group functional was done. The tested method gives the following quantum parameters of energy gap (ΔE), fraction of electron transfer (ΔN), dipole moment (μ), absolute electronegativity (χ), ionization energy (I), hardness (η), and softness (σ) for the prepared compounds L400 and L600 in both gas and solvated phases. The adsorption energy of the tested compound on Fe is induced from the MC simulation with the aid of the adsorption locator module in the same software. The MC simulation has been done in gas and solution simulated phases of the tested acidic (HCl) medium.[26,27]

3. RESULTS AND DISCUSSION

3.1. Tafel. The electrochemical kinetic parameters of the corrosion and corrosion inhibition of the X65 carbon steel have been obtained from the Tafel polarization data in the absence and presence of different concentrations of the prepared nonionic surfactant compounds, which have different in an in situ number of ethylene oxide units (L400 and L600) are exported from Figure 1a1,a2.

Figure 1a represents the relation between the carbon steel corrosion potential (E_{mV}) vs the Ag/AgCl reference electrode and log I_{corr} (corrosion current density) in 1 M HCl in the absence and presence of different concentrations of L400 and L600. From Figure 1a, it can be seen that the addition of L400 and L600 shifts the anodic/cathodic polarization curves toward the noble direction, indicating a decrease in the corrosion rate of the tested alloy.[28] Not to mention, with the addition of the prepared nonionic surfactant molecules, the corrosion potential changed within ±85 mV towards the blank one, and this indicates that these tested inhibitors act as mixed-type inhibitors.[29]

The electrochemical parameters obtained from Figure 1a, such as i_{corr}, E_{corr}, β_a, and β_c, are tabulated in Table 1. In addition to that, the surface coverage (θ) and the inhibition efficiency percentage (IE (%)) are calculated according to eqs 2 and 3 and tabulated in Table 1.

The close inspection of Table 1 declares that the addition of inhibitors has a huge effect on the corrosion current density and corrosion rate even in low concentrations. i_{corr} is dramatically decreased compared to the blank. This refers to the adsorption ability of the prepared inhibitors due to the presence of high-electron-density centers (O, N, and π electrons). Corrosion rate (mpy) can be calculated using the corrosion current density according to eq 5

$$\text{CR} = \frac{0.129 \times \text{eq. wt.} \times i_{corr}}{d} \quad (5)$$

where eq. wt., d, and i_{corr} are the current equivalent weight, the iron density, and the corrosion current density, respectively.[30] Furthermore, the corrosion current density and CR decrease with both concentrations of inhibitor and the number of ethylene oxide units (L400 < L600), as shown in Figure 1b. Furthermore, the polarization resistance calculated using the Stern−Geary equation (eq 6) and tabulated in Table 1

$$R_p = \frac{[(\beta_a \cdot \beta_c)/2.303(\beta_a + \beta_c)]}{I_{corr}} \quad (6)$$

where β_a and β_c are the slopes of the anodic and cathodic Tafel, respectively. The polarization resistance value is inversely proportional to the corrosion current density. The R_p increases from 79 to 569 Ω·cm^2 with the increasing concentration from 1 × 10^{-6} to 1 × 10^{-4} M of the added inhibitor L400. Also, it increases from 569 to 630 Ω·cm^2 as the number of ethylene oxide units increase for L600 at the same concentration (1 ×

https://dx.doi.org/10.1021/acsomega.0c05476
ACS Omega 2021, 6, 4300−4312

10^{-4} M). The potentiodynamic polarization values agree with R_{ct} values obtained from EIS, which will be discussed later.[31,32] The adsorption of the inhibitor molecule over the X65 surface increases the surface coverage and, in turn, decreases the dissolution rate of X65. The order of the inhibition efficiency of the prepared compounds is (L400 < L600).

3.2. EIS. The nondestructive electrochemical impedance spectroscopy (EIS) test method is used to evaluate the performance of the tested corrosion inhibitor compounds for the X65 steel in 1 M HCl at room temperature. Nyquist and Bode plots for X65 in 1 M HCl in the absence and the presence of different concentrations of the prepared nonionic surfactants differ in an in situ number of ethylene oxide units represented the EIS performance of the X65 steel corrosion in acidic media are shown in Figures 2 and 3. The Nyquist curves show the

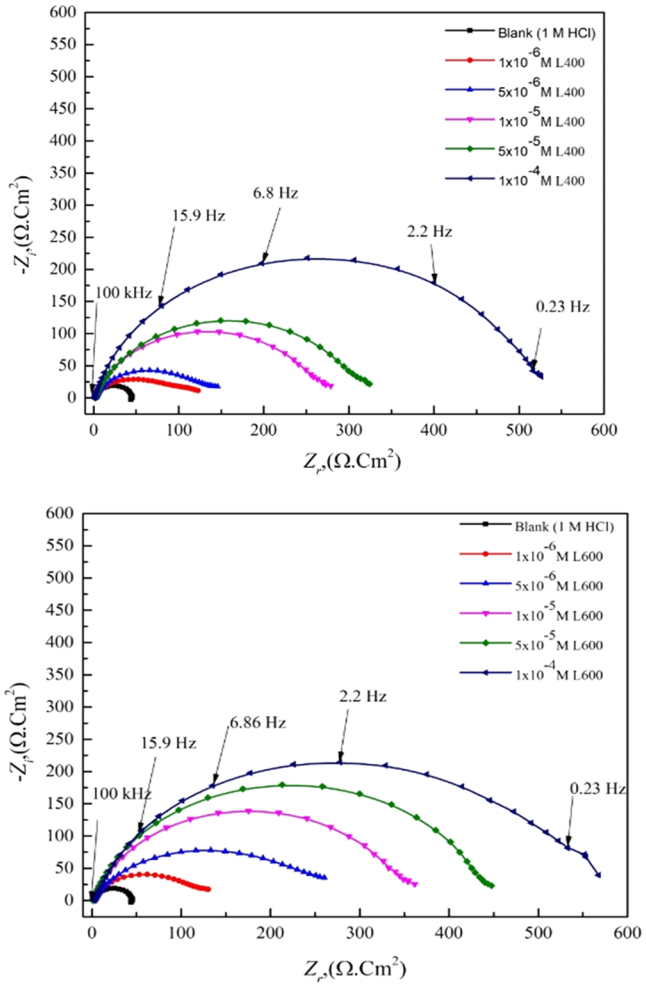

Figure 2. EIS Nyquist plot of the X65 steel in 1 M HCl with various concentrations of L400 and L600 at 25 °C.

depressed semicircles under the real axis with one time constant, as shown in bode plots; this indicates that the charge transfer process controls the X65 corrosion process.[33] The depressed shape of the Nyquist plot is due to the frequency depression phenomenon that returned into the inhomogeneity of the electrode surface.[34] The overall shape of the EIS diagrams (Nyquist and Bode) of X65 in 1 M HCl before and after the inhibitor addition are not changed; this suggested that the X65 dissolution reaction mechanism controlled by the charge

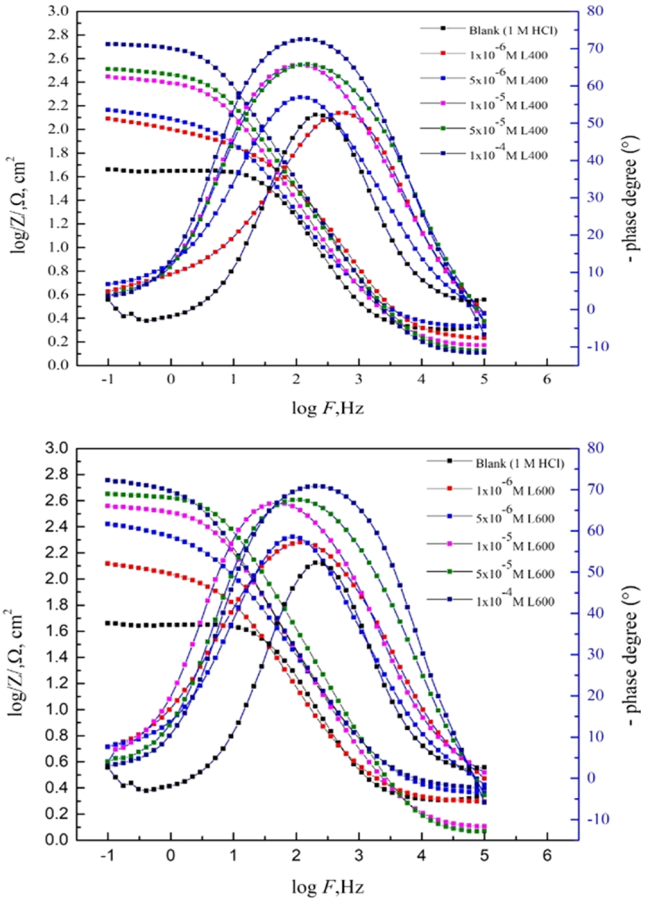

Figure 3. EIS bode for the X65 steel in 1 M HCl in the presence of different concentrations of L400 and L600 at 25 °C.

transfer process is neither changed or nor affected by inhibitor addition.[35]

The addition of the tested compounds leads to an increase in the diameter of the Nyquist plot (as seen in Figure 2), shift in the /Z/ at the lower-frequency region to a higher value, and shift in the phase-angle value toward −90 °C at an intermediate frequency region (as presented in the bode plots; Figure 3). This is related to the inhibitor adsorption over the X65 surface.[36,37] The EIS experimental data can be fitted using a simple Randles equivalent circuit that is composed of R_s, electrolyte (solution) resistance, R_{ct}, Fe ion transfer resistance, and constant phase element (CPE) parameter Y_0 in place of C_{dl} (double-layer capacitance) to obtain more fitted simulated data. Figure 4 shows the blank and high concentration (1×10^{-4} M) from both compounds as representative concentrations fitted with the proposed equivalent circuit in situ.

The EIS parameters obtained are tabulated in Table 2. The addition of nonionic surfactants with different ethylene oxide units even in low doses has a great effect on the R_{ct} value, as shown in Table 2.

Increasing both the concentration and ethylene oxide unit increases the X65 surface coverage, which, in turn, leads to an increase in the charge-transfer resistance.[38] Also, the addition of inhibitor leads to the decrease in the double-layer capacitance C_{dl} values recorded in Table 2, as the protective layer formed (over X65 surface) by the tested compounds have lower dielectric constant values compared with the replaced adsorbed water and aggressive chloride ion counterparts.[39] Figure 5 represents the relationship between the inhibitor dose of both

https://dx.doi.org/10.1021/acsomega.0c05476
ACS Omega 2021, 6, 4300−4312

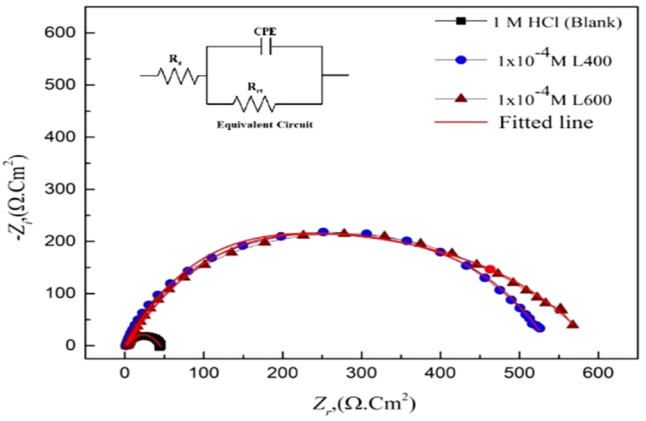

Figure 4. Nyquist plot of X65 steel in absence and presence 1×10^{-4} M of L400 and L600 using the proposed in situ equivalent circuit.

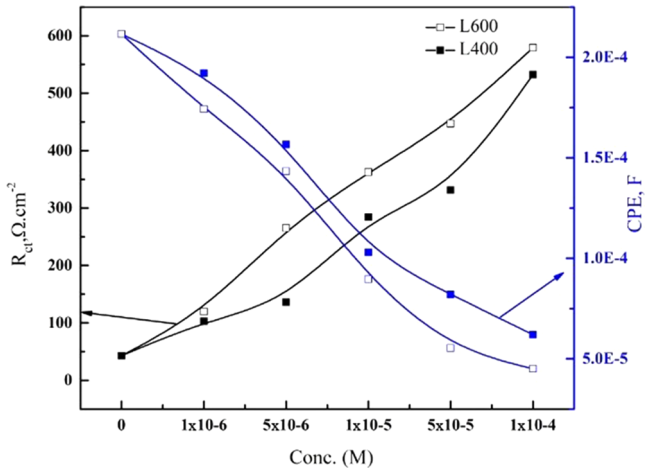

Figure 5. Relation between R_{ct}, CPE, and inhibitor concentrations of different ethylene oxide units.

the used inhibitors differ in in situ number of ethylene oxide units and R_{ct} and C_{dl}. It can be said that the corrosion inhibition order is related to the molecular weight of the tested compound (L400 < L600), and this is matched with the previously discussed potentiodynamic polarization data.

3.3. Adsorption Isotherm. Competitive adsorption process occurring at the electrode/electrolyte interface between the inhibitor molecules and the water or/and Cl^- ion is controlled by the quasi-substitution process according to eq 7

$$EO_{sol} + nH_2O/Cl_{ads} \leftrightarrow EO_{ads} + nH_2O_{sol} \quad (7)$$

where EO_{sol} and EO_{ads} are the ethylene oxide molecules in the aqueous solution and adsorbed on the metallic surface, respectively. The protective shielded layer covering the electrode surface (θ) is related to the adsorption phenomenon. Different adsorption isotherm models such as Temkin, Frumkin, Flory–Huggins, and Langmuir are used to fit the Tafel and the EIS data via the relation between the inhibitor concentration (C_{inh}) and the surface coverage (θ). Based on the high correlation coefficient (R^2), the more fitted adsorption model was found Langmuir adsorption isotherm (as shown in Figure 6) that describes the inhibitor adsorption process faultlessly according to[40,41]

$$\frac{C}{\theta} = \frac{1}{K_{ads}} + C \quad (8)$$

where θ is the surface coverage, K_{ads} is the adsorption constant, and C is the inhibitor concentration. The inhibitor adsorption free energy (ΔG_{ads}) was calculated with the help of (K_{ads}) value according to eq 9

$$\Delta G_{ads} = \left(\frac{1}{55.5}\right) \exp(-k_{ads}/RT) \quad (9)$$

where the molar concentration value of water was 55.5 M and R is the gas constant under standard conditions.

The values of ΔG_{ads} and K_{ads} are recorded in Table 3. The higher value of K_{ads} indicates the adsorption strength of the inhibitor, and the negative sign of ΔG_{ads} points to the spontaneity of the adsorption process. The higher ΔG_{ads} values recorded in Table 3 indicate that the chemical adsorption behavior of the prepared compound, which occurs via the transfer of electrons from high electron centers to the vacant 3d orbital of Fe, forming a covalent bond. The negative value of the adsorption free energy charge increases with the increasing molecular weight of the tested compounds (from −43.22 to −45.16 for L400 and L600), and this is matched with the potentiodynamic and the EIS data.[42,43]

3.4. SEM and EDX Analysis. Surface analysis studies (SEM and EDX) for the X65 steel slides immersed for 3 h in a pure solution of 1 M HCl and the other treated with optimum concentration (1×10^{-4} M) of the best tested nonionic

Table 2. Electrochemical Parameters of the Impedance of the X65 Steel in 1 M HCl in the Absence and Presence of Various Concentrations of the L400 and L600 Nonionic Surfactants at 25 °C

				CPE			
	conc. (M)	R_s (Ω·cm^2)	R_{ct} (Ω·cm^2)	CPE (μF)	C_{dl} (F)	N	θ	IE (%)
blank	0.00	2.0121	42.6	2.115×10^{-4}	0.587	0.7861		
L400	1×10^{-6}	1.2371	102.76	1.9202×10^{-4}	0.675	0.7898	0.58544	58.54
	5×10^{-6}	1.6935	136.16	1.5658×10^{-4}	0.634	0.8098	0.6871	68.71
	1×10^{-5}	1.5089	284.35	1.0297×10^{-4}	0.555	0.8511	0.8501	85.01
	5×10^{-5}	1.326	331.17	8.1964×10^{-5}	0.373	0.8210	0.8713	87.13
	1×10^{-4}	0.73274	532.4	6.2021×10^{-5}	0.312	0.8325	0.9199	91.99
L600	1×10^{-6}	1.9861	119.62	1.7422×10^{-4}	0.633	0.7928	0.6438	64.38
	5×10^{-6}	1.8153	265.12	1.4336×10^{-4}	0.619	0.8107	0.8393	83.93
	1×10^{-5}	1.5884	362.68	8.9572×10^{-5}	0.484	0.8481	0.8825	88.25
	5×10^{-5}	1.1883	446.85	5.5337×10^{-5}	0.265	0.8345	0.9046	90.46
	1×10^{-4}	1.2608	579.27	4.5035×10^{-5}	0.237	0.8510	0.9264	92.64

https://dx.doi.org/10.1021/acsomega.0c05476
ACS Omega 2021, 6, 4300−4312

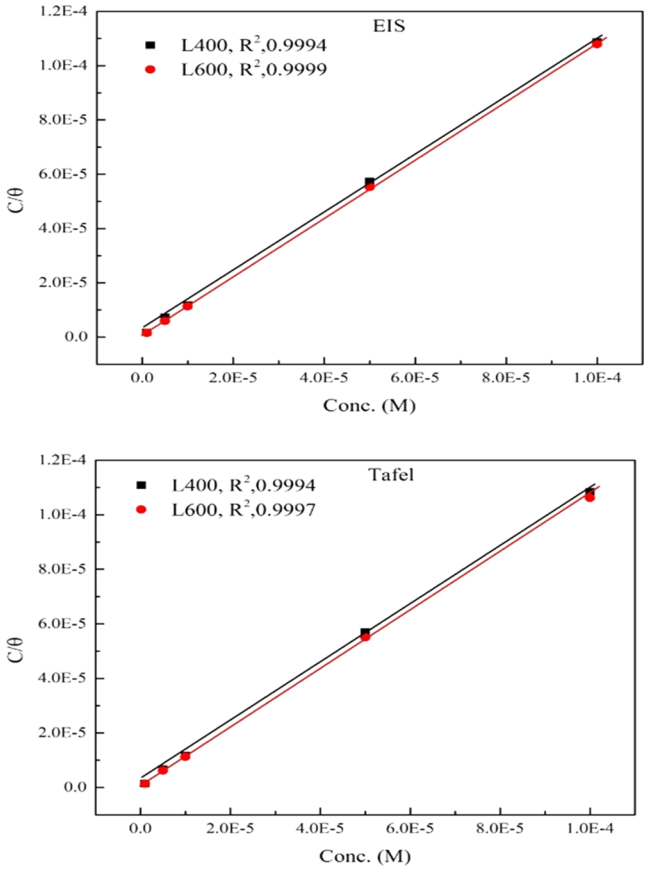

Figure 6. Langmuir isotherm adsorption model of L400 and L600 on the X65 steel surface in 1 M HCl at 25 °C from the EIS and Tafel measurements.

Table 3. Langmuir Isotherm Parameters for the Adsorption of the Synthesized Inhibitors on the X65 Steel Surface in 1 M HCl at 25 °C from the EIS and Tafel Measurements

		method	
inhibitor	parameter	Tafel	EIS
L400	R^2	0.9994	0.9994
	slope	1.08	1.08
	K (L·mg^{-1}) × 10^5	8.60	6.79
	$-\Delta G$ (kJ·mol^{-1})	43.81	43.22
L600	R^2	0.9997	0.9999
	slope	1.05	1.07
	K (L·mg^{-1}) × 10^5	12.01	14.80
	$-\Delta G$ (kJ·mol^{-1})	44.64	45.16

surfactant compound (L600) have been represented in Figures 7 and 8, respectively. SEM analysis technique gives the two-dimensional (2D) visual information about the performance of the insight inhibitor toward the metal corrosion. From Figure 7, it can be observed that the higher damage X65 surface fulfilled with corrosion product while, with Figure 8, after adding the optimum concentration of L600, the X65 surface becomes more smooth and free somewhat from corrosion product this inferred the inhibition action of L600 via blocking the active centers of the metal surface.[44] EDX gives the chemical composition of the outer layer surface of X65 in the absence and presence of 1 × 10^{-4} M of L600 in 1 M HCl. The peak intensity of Fe higher in the absence of an inhibitor while a decrease in the presence of inhibitor confirms the shielding X65 surface with protecting inhibitor and decrease with corrosion product. The (−N−) atom peak appearance in the presence of inhibitor indicates the formation of the protective adsorbed layer. These observations are in agreement with the previously published data.[45−47]

3.5. Quantum Chemical Calculation. The adsorption ability of the prepared nonionic surfactants L400 and L600 over the X65 steel surface can be discussed from a quantum chemical calculation point of view via frontier molecular orbital theory (FMOT) and Monte Carlo simulation with the aid of Material Studio software (MS 6.0, Accelrys).[48] The adsorption of the tested inhibitors could be based on the donor−acceptor interaction phenomena. In that case, the electrons are transferred from the high-electron-density centers (O, N, and π electrons, i.e., regions of highly electronic distributions) of the organic compounds to the vacant 3d orbital of the metal (iron). The quantum chemical parameters obtained from the optimization of L400 and L600 in the gas and solvent phases (shown in Figure 9a,b) are depicted in Table 4 and discussed as follows. The energy of the highest occupied molecular orbital (E_{HOMO}) represents the electron-donating ability of the tested compounds. The lower value of E_{LUMO} indicates the ability of the molecules to accept the electrons from the back donation of Fe and thus increase the binding energy between the metal and the inhibitor.

The higher E_{HOMO} and the lower E_{LUMO}, the higher the adsorption/binding ability of the tested inhibitor with the metal surface.[20,49−53] E_{HOMO} increases with increasing the ethylene oxide units, as presented in Table 4. This is in good agreement with the experimental data, suggesting that L600 is better than L400.[54] The chemical reactivity is controlled by the energy gap ΔE_{gap} values. From the reactivity point of view, the higher inhibition performance molecule is the higher reactive ones toward the substrate surface, and the most stable ones is the lower ΔE_{gap}. Therefore, L600 forms a more stable complex with the Fe substrate rather than L400. The dipole moment (μ) results from nonuniform charge distribution over the atoms in the molecule. Decreasing in the dipole moment values support inhibitor molecule accumulation over the Fe surface and thus increase the adsorption ability of L600 over that of L400 as well as matched with the experimental data.[55,56] The absolute electronegativity (χ), hardness (η), softness (σ), and fraction of electron transfer (ΔN) collectively represent the active parameters that are calculated from eqs 10 to 13

$$\chi = \frac{I + A}{2} \tag{10}$$

$$\eta = \frac{I - A}{2} \tag{11}$$

$$\sigma = \frac{1}{\eta} \tag{12}$$

$$\Delta N = \frac{(\chi_{Fe} - \chi_{inh})}{2\,(\eta_{Fe} - \eta_{inh})} \tag{13}$$

where I is the ionization energy ($I = -E_{HOMO}$) and A is the electron affinity ($A = -E_{LUMO}$).

According to the concept of the hard−soft acid−base, the soft molecule has lower values of ΔE_{gap} and higher basicity and vice versa compared with the hard ones.[57] Therefore, the soft molecule has adsorption ability due to the ease of electron transfer compared to the hard one and the better corrosion inhibitor. According to Lukovit's study, the inhibition perform-

https://dx.doi.org/10.1021/acsomega.0c05476
ACS Omega 2021, 6, 4300−4312

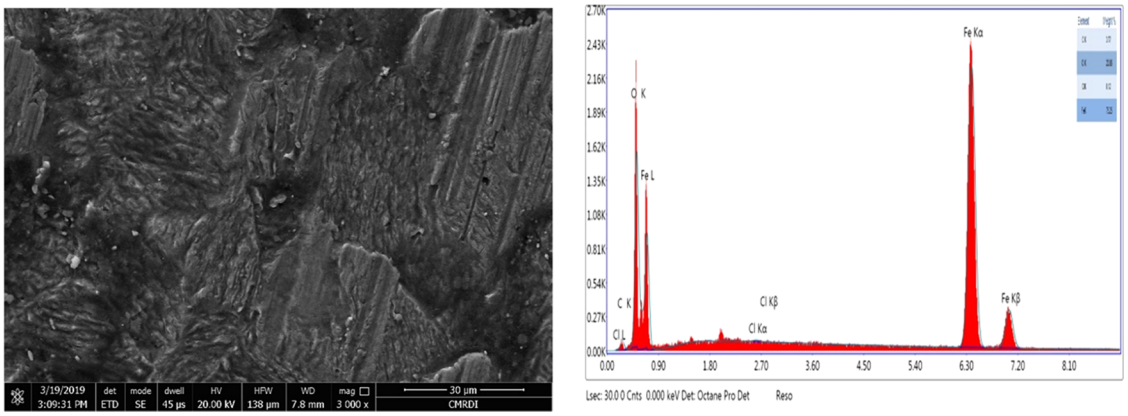

Figure 7. SEM surface analysis micrograph of the X65 steel immersed in 1 M HCl at 25 °C for 3 h and the EDX analysis for the X65 steel blank quantification of the elements present.

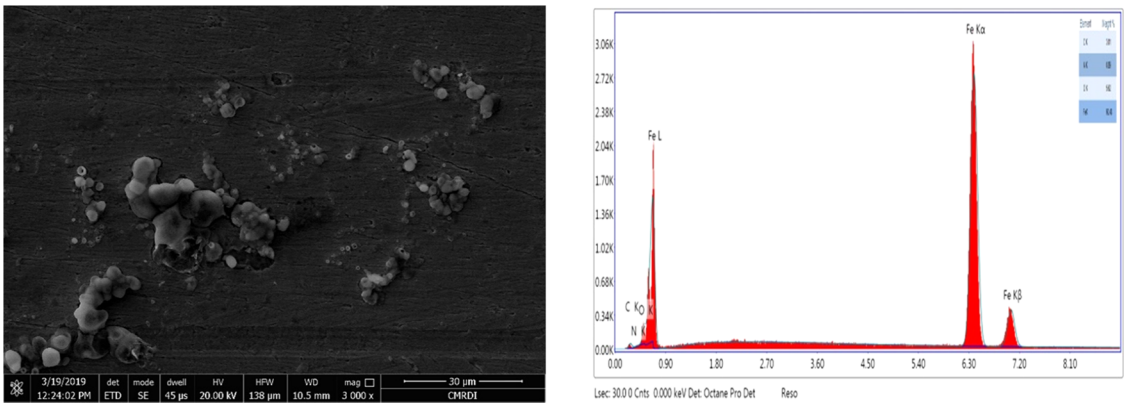

Figure 8. SEM surface analysis micrograph of the X65 steel after the addition of 1×10^{-4} M L600 at 25 °C for 3 h and the EDX analysis for the X65 steel and quantification of elements present.

ance as a function of electron transfer increases when the number of electrons transferred (ΔN) is less than 3.6.[27]

The higher the fraction of electron transfer (ΔN), the better is the corrosion inhibitor. ΔN increases as the number of ethylene oxide units increase, as reported in Table 4, and this confirms the highest electroadsorption ability of L600 compared to L400 as previously declared by the experimental data. Ionization energy represents the chemical reactivity of atoms and molecules. Therefore, as the ionization energy increases, the reactivity increases and, in turn, the inhibition efficiency decreases (L400 < L600).[58] These support the obtained electrochemical data (Tafel and EIS).

3.6. Monte Carlo Simulations. The MC simulations for both L400 and L600 in the gas phase and solution simulated the acidic medium with 500 H_2O/5 Cl^-/5 H_3O^+ were introduced to simulate the real corrosive medium has been executed using adsorption locator module via the following system:

(A) Fe (1 1 0) crystal, the metal, is considered in the recent study, as the most stable surface was used in the simulation process.

(B) Cleavage plane (35 × 35) supercell.

(C) 30 Å vacuum slab to remove the periodic boundary effect.

MC simulation gives us a good image of the orientation and interaction between the prepared compounds over the Fe surface, as shown in Figure 10a,b. Both L400 and L600 are oriented horizontally and parallel to the Fe crystal (1 1 0) surface to maximize the contact and increase the surface coverage, which achieves higher adsorption energy and reflects a higher inhibition efficiency.

From Table 5, it is obvious that E_{ads} for L600 on the Fe (1 1 0) in the presence of H_2O and HCl is greater than that for L400 due to a higher number of electron-donating (ethylene oxide) units and achieves a higher inhibition efficiency. The higher adsorption energy of the molecules indicates the ability of the tested compound to replace the corrosive ions and H_2O molecules to form a protective shield layer against the corrosive medium.[27,39]

4. MECHANISM OF CORROSION INHIBITION ON X65 STEEL

The inhibition inertia of organic molecules originated from the formation of a protective layer that is absorbed on the iron surface. Both the electrochemical and microscopic measurements confirmed that the corrosion of the X65 steel was meaningfully reduced in the presence of inhibitors (L400 and L600). Additionally, the adsorption isotherm studies prove that the adsorption of the inhibitors over the iron surface is highly fitted to the Langmuir adsorption model. Besides, the adsorption behavior of the formed protective film is primarily achieved by (1) the electrostatic interaction via the protonated heteroatoms and (2) various bonds between the inhibitor molecules and the X65 steel surface. More precisely, the interaction between the inhibitors (L400 and L600) and the X65 steel surface is shown in Figure 11. There are two predominant adsorption methods between the inhibitor molecule and the

https://dx.doi.org/10.1021/acsomega.0c05476
ACS Omega 2021, 6, 4300−4312

a

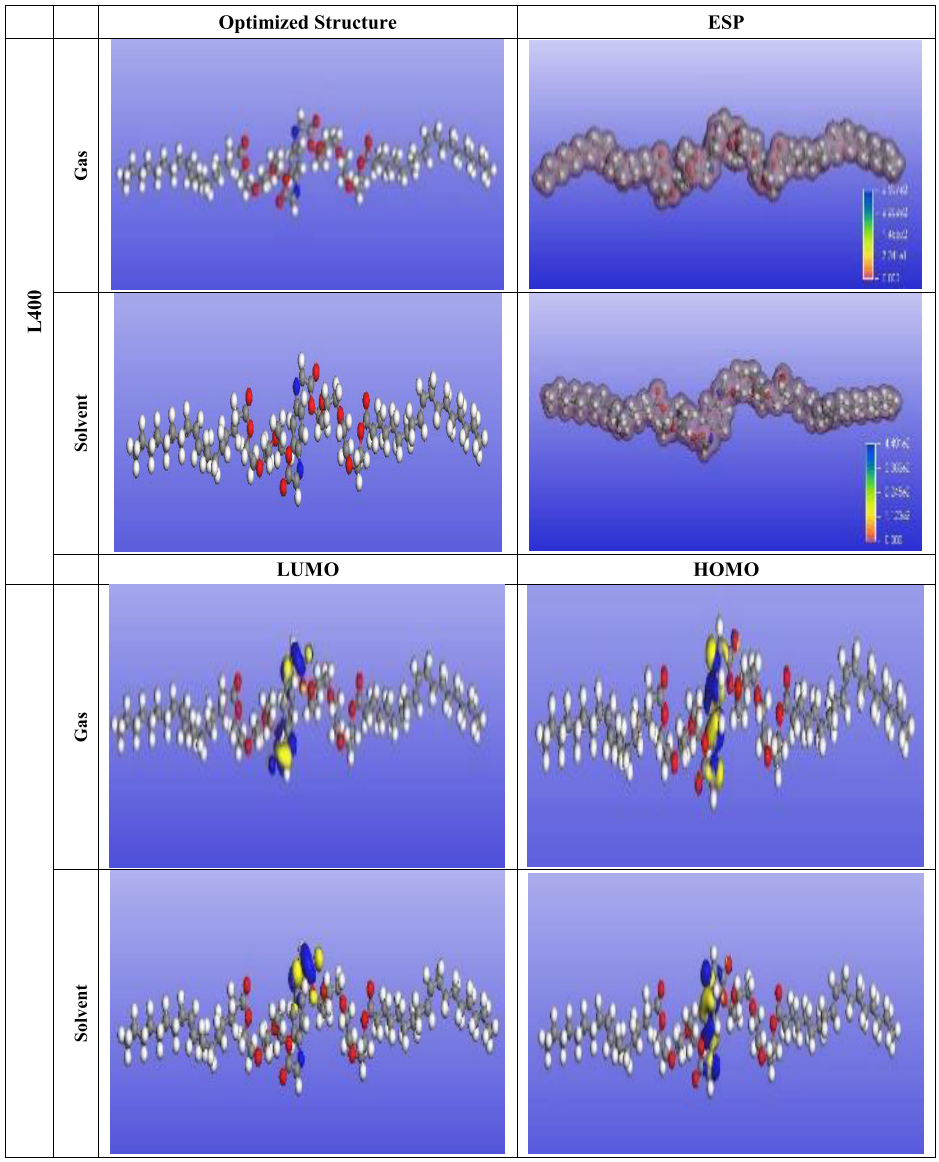

Figure 9. continued

https://dx.doi.org/10.1021/acsomega.0c05476
ACS Omega 2021, 6, 4300−4312

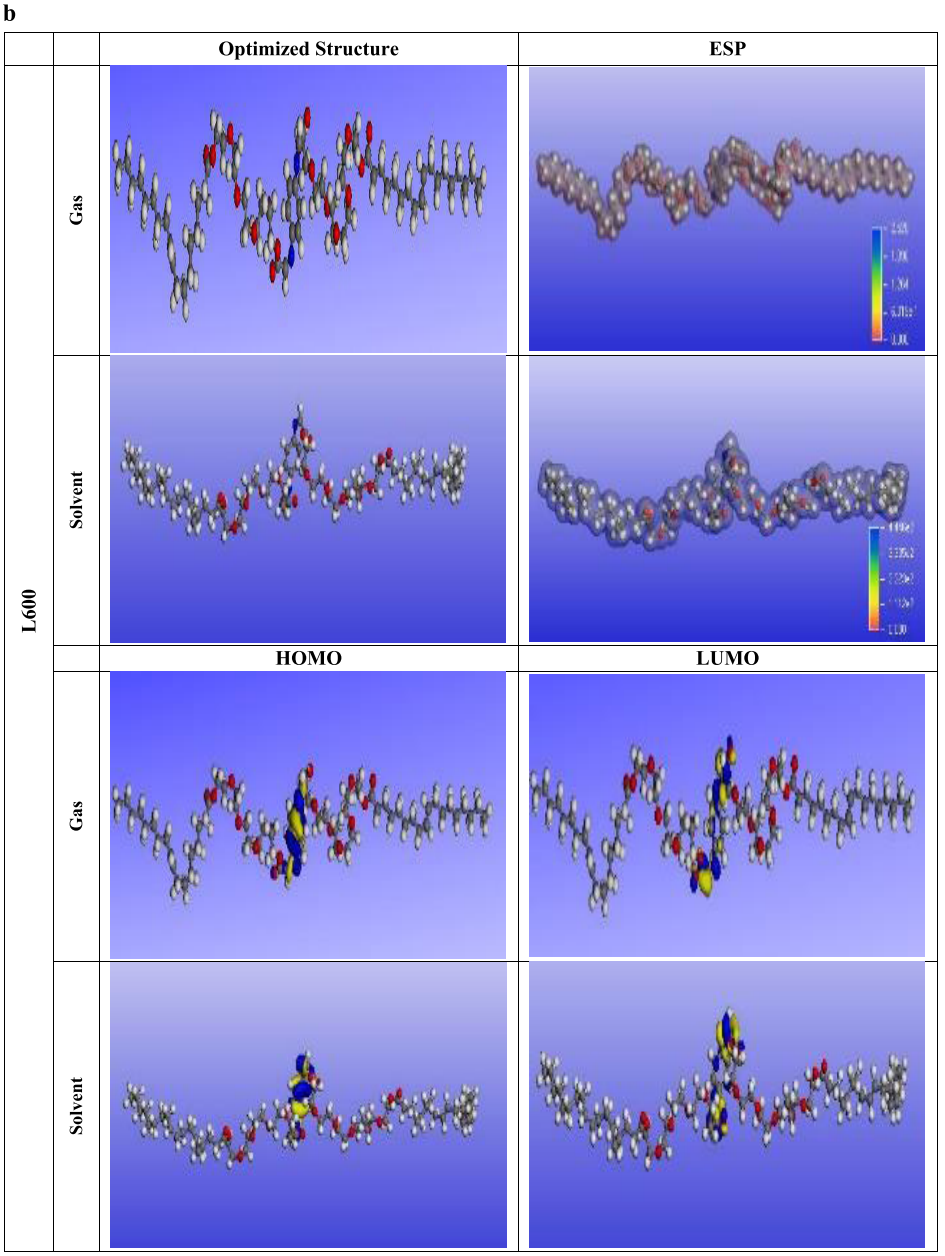

Figure 9. (a) Optimized structures, highest occupied molecular orbitals (HOMO), lowest unoccupied molecular orbitals (LUMO), and molecular electrostatic potential maps of the synthesized L400. (b) Optimized structures, highest occupied molecular orbitals (HOMO), lowest unoccupied molecular orbitals (LUMO), and molecular electrostatic potential maps of the synthesized L600.

Table 4. Quantum Chemical Parameters of the Investigated Inhibitors

inhibitor		E_{HOMO}	E_{LUMO}	ΔE (eV)	A	I	χ (eV)	η (eV)	ΔN (eV)	μ (D)
L400	gas	−4.2812	−1.998	2.2827	1.998	4.2812	3.1399	1.141	1.1413	4.9768
	solvent	−4.6104	−2.361	2.2492	2.361	4.6104	3.4858	1.124	1.5623	9.7372
L600	gas	−4.2648	−2.340	1.9242	2.340	4.2648	3.3027	0.962	1.9213	4.3482
	solvent	−4.5482	−2.321	2.2271	2.321	4.5482	3.4346	1.113	1.6008	8.9902

X65 surface: first, the interaction between the π-electrons of the benzene ring and the unoccupied d-orbital of the Fe atoms; second, the donor−acceptor interactions between the vacant d-orbital of the iron (X65 steel) surface atoms and the lone electron pairs in the heteroatoms (N and O). These active electrons are disposed to be shared with the d-orbitals of the Fe atom.

5. CONCLUSIONS

(1) The synthesized ethoxylated nonionic surfactants have high corrosion inhibition performance in the X65 steel in 1 M HCl due to the presence of the highly effective electronic adsorption centers (O, N, and π-bond) that block the active centers of iron metal.

https://dx.doi.org/10.1021/acsomega.0c05476
ACS Omega 2021, 6, 4300−4312

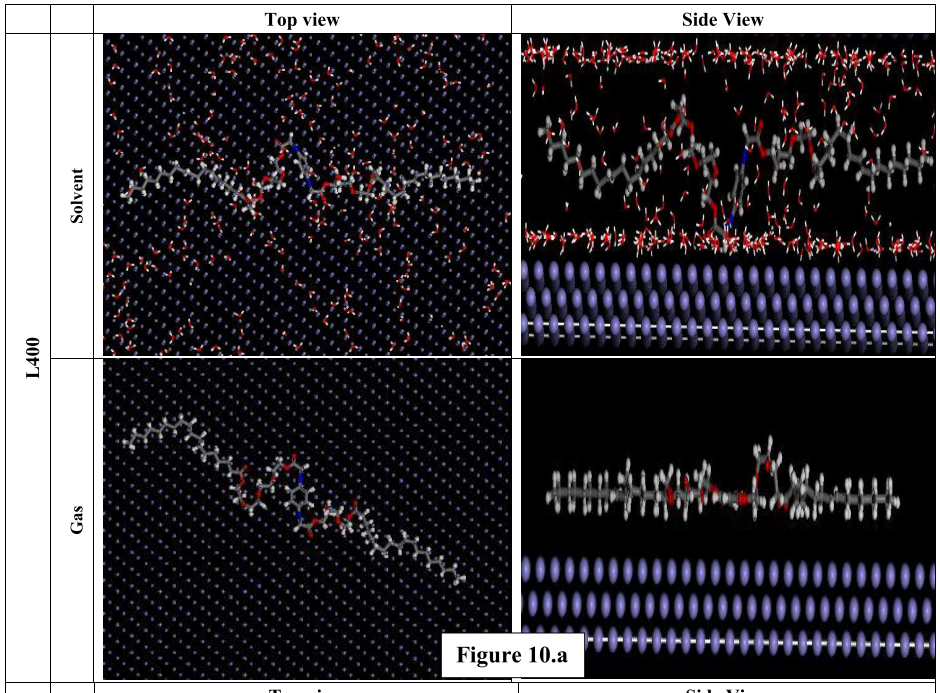

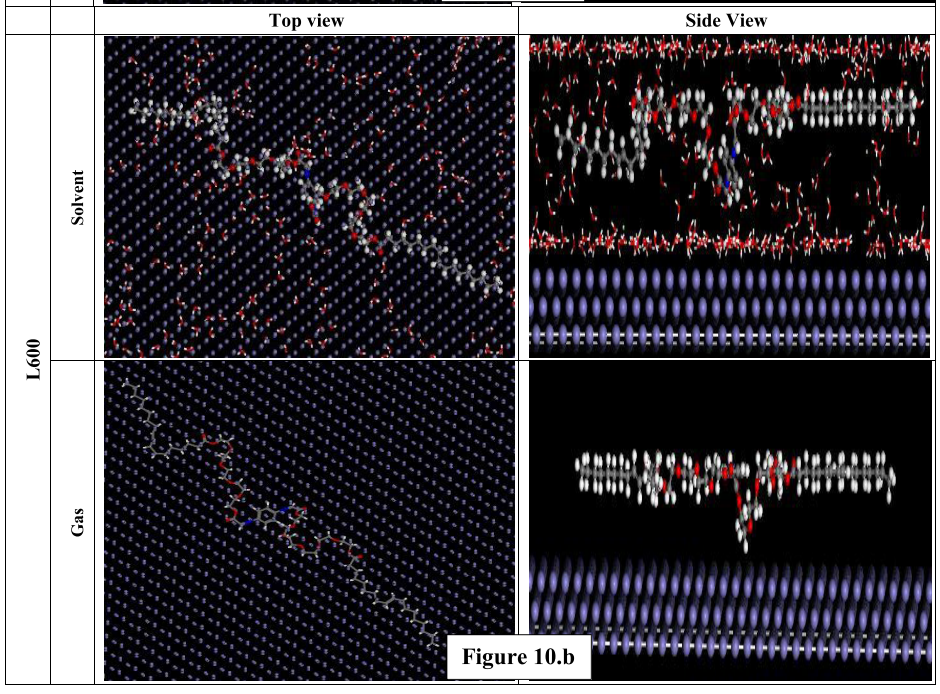

Figure 10. (a) Top (left) and side (right) views of the most stable low-energy configurations for the adsorption of L400 on the Fe (1 1 0) in a vacuum and a simulated solution (500 H_2O/5 Cl^-/5 H_3O^+) phases obtained using the Monte Carlo simulations. (b) Top (left) and side (right) views of the most stable low-energy configuration for the adsorption of L600 on the Fe (1 1 0) in a vacuum and a simulated solution (500 H_2O/5 Cl^-/5 H_3O^+) phases obtained using the Monte Carlo simulations.

Table 5. Output Energies Calculated by Monte Carlo Simulations for the Prepared Compounds in Gas and Solution Phases on the Fe (1 1 0)

compound	total energy (kJ/mol)	adsorption energy (kJ/mol)	rigid adsorption energy (kJ/mol)	deformation energy (kJ/mol)	(dE_{ads}/d_{Ni}) (kJ/mol)	H_2O:dE_{ad}/d_{Ni}	H_3O^+:dE_{ad}/d_{Ni}	Cl^-:dE_{ad}/d_{Ni}
L400 gas	−670.09	−741.91	−594.728	−147.182	−741.91			
L400 + 5 HCl + 500 H_2O	-6.57×10^3	-1.65×10^4	-6.68×10^3	-9.78×10^3	−555.947	−19.85	−116.81	−76.022
L600 gas	−763.809	−798.002	−662.044	−135.958	−798.002			
L600 + 5 HCl + 500 H_2O	-6.69×10^3	-1.66×10^4	-6.78×10^3	-9.77×10^3	−643.178	−20.08	−185.35	−122.98

https://dx.doi.org/10.1021/acsomega.0c05476
ACS Omega 2021, 6, 4300−4312

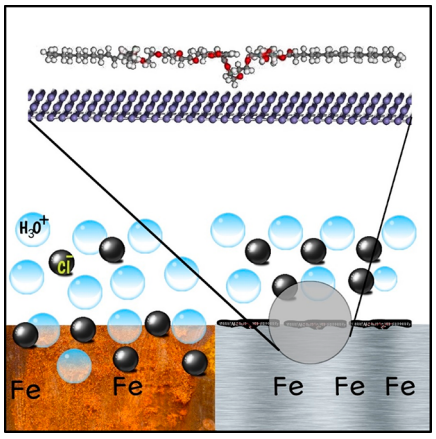

Figure 11. Simulated corrosion and corrosion inhibition reaction mechanism of X65 in 1 M HCl in the absence and presence of the tested nonionic surfactants.

(2) The EIS and Tafel electrochemical techniques showed that the inhibition efficiency increases with increasing both the concentration and the ethoxylation degree; therefore, the IE (%) for L600 is higher than that of L400 over the whole concentrations used.
(3) The potentiodynamic polarization (PDP) data suggest the mixed-type behavior of the tested inhibitors as the change in E_{corr} was within ±85 mV around E_{ocp} of the blank.
(4) MC simulation clarifies that the adsorption energy of the inhibitor molecule over the X65 steel was more than those of the water molecule and chloride ions and agrees with the decrease in C_{dl} as a result of the adsorption of inhibitor over the X65 surface in place of water and aggressive ions.

AUTHOR INFORMATION

Corresponding Authors

Mohamed Abd El-raouf − *Egyptian Petroleum Research Institute (EPRI), 11727 Cairo, Egypt; National Alliance of Petrochemicals, EPRI, 11727 Cairo, Egypt;* orcid.org/0000-0001-8258-5425; Email: abdelraouf1979@yahoo.com

N. M. El Basiony − *Egyptian Petroleum Research Institute (EPRI), 11727 Cairo, Egypt; National Alliance of Petrochemicals, EPRI, 11727 Cairo, Egypt;* Email: n.elbasiony56@gmail.com

Authors

Ahmed G. Bedir − *Egyptian Petroleum Research Institute (EPRI), 11727 Cairo, Egypt; National Alliance of Petrochemicals, EPRI, 11727 Cairo, Egypt*

Samah Abdel-Mawgoud − *Chemistry Department, Faculty of Science, Benha University, 13511 Benha, Egypt*

Nabel A. Negm − *Egyptian Petroleum Research Institute (EPRI), 11727 Cairo, Egypt; National Alliance of Petrochemicals, EPRI, 11727 Cairo, Egypt*

Complete contact information is available at: https://pubs.acs.org/10.1021/acsomega.0c05476

Notes

The authors declare no competing financial interest.

ACKNOWLEDGMENTS

Support of this work by the Egyptian Petroleum Research Institute is gratefully acknowledged.

REFERENCES

(1) Badr, G. E. The role of some thiosemicarbazide derivatives as corrosion inhibitors for C-steel in acidic media. *Corros. Sci.* **2009**, *51*, 2529−2536.
(2) Kaczerewska, O.; Leiva-Garcia, R.; Akid, R.; Brycki, B. Efficiency of cationic gemini surfactants with 3-azamethylpentamethylene spacer as corrosion inhibitors for stainless steel in hydrochloric acid. *J. Mol. Liq.* **2017**, *247*, 6−13.
(3) Behpour, M.; Ghoreishi, S. M.; Khayatkashani, M.; Soltani, N. Green approach to corrosion inhibition of mild steel in two acidic solutions by the extract of Punica granatum peel and main constituents. *Mater. Chem. Phys.* **2012**, *131*, 621−633.
(4) Goyal, M.; Kumar, S.; Bahadur, I.; Verma, C.; Ebenso, E. E. Organic corrosion inhibitors for industrial cleaning of ferrous and non-ferrous metals in acidic solutions: A review. *J. Mol. Liq.* **2018**, *256*, 565−573.
(5) Saha, S. K.; Dutta, A.; Ghosh, P.; Sukul, D.; Banerjee, P. Novel Schiff-base molecules as efficient corrosion inhibitors for mild steel surface in 1 M HCl medium: experimental and theoretical approach. *Phys. Chem. Chem. Phys.* **2016**, *18*, 17898−17911.
(6) Chauhan, D. S.; Quraishi, M.; Sorour, A.; Saha, S. K.; Banerjee, P. Triazole-modified chitosan: a biomacromolecule as a new environmentally benign corrosion inhibitor for carbon steel in a hydrochloric acid solution. *RSC Adv.* **2019**, *9*, 14990−15003.
(7) Sukul, D.; Pal, A.; Saha, S. K.; Satpati, S.; Adhikari, U.; Banerjee, P. Newly synthesized quercetin derivatives as corrosion inhibitors for mild steel in 1 M HCl: combined experimental and theoretical investigation. *Phys. Chem. Chem. Phys.* **2018**, *20*, 6562−6574.
(8) Elwan, H. A.; Zaky, M. T.; Farag, A. S.; Soliman, F. S.; Ezel Dean Hassan, M. A coupled extractive-oxidative process for desulfurization of gasoline and diesel fuels using a bifunctional ionic liquid. *J. Mol. Liq.* **2017**, *248*, 549−555.
(9) Dutta, A.; Saha, S. K.; Banerjee, P.; Patra, A. K.; Sukul, D. Evaluating corrosion inhibition property of some Schiff bases for mild steel in 1 M HCl: competitive effect of the heteroatom and stereochemical conformation of the molecule. *RSC Adv.* **2016**, *6*, 74833−74844.
(10) Singh, A.; Ansari, K.; Quraishi, M.; Kaya, S.; Banerjee, P. The effect of an N-heterocyclic compound on corrosion inhibition of J55 steel in sweet corrosive medium. *New J. Chem.* **2019**, *43*, 6303−6313.
(11) Tripathy, D. B.; Murmu, M.; Banerjee, P.; Quraishi, M. A. Palmitic acid based environmentally benign corrosion inhibiting formulation useful during acid cleansing process in MSF desalination plants. *Desalination* **2019**, *472*, No. 114128.
(12) Al-Abdali, F. H.; Abdallah, M.; El-Sayed, R. Corrosion inhibition of aluminum using nonionic surfactant compounds with a six membered heterocyclic ring in 1.0 M HCl solution. *Int. J. Electrochem. Sci.* **2019**, *14*, 3509−3523.
(13) Fouda, A. S.; El-Askalany, A.; El-Habab, A.; Ahmed, S. Anticorrosion Properties of Some Nonionic Surfactants on Carbon Steel in 1 M HCl Environment. *J. Bio- Tribo-Corros.* **2019**, *5*, 56.
(14) Shaban, S. M.; Abd-Elaal, A. A.; Tawfik, S. M. Gravimetric and electrochemical evaluation of three nonionic dithiol surfactants as corrosion inhibitors for mild steel in 1 M HCl solution. *J. Mol. Liq.* **2016**, *216*, 392−400.
(15) Al-Sabagh, A. M.; Nasser, N. M.; El-Azabawy, O. E.; Tabey, A. E. E. Corrosion inhibition behavior of new synthesized nonionic surfactants based on amino acid on carbon steel in acid media. *J. Mol. Liq.* **2016**, *219*, 1078−1088.
(16) Abdallah, M.; Al Jahdaly, B.; Al-Malyo, O. Corrosion inhibition of carbon steel in hydrochloric acid solution using non-ionic surfactants derived from phenol compounds. *Int. J. Electrochem. Sci.* **2015**, *10*, 2740−2754.

https://dx.doi.org/10.1021/acsomega.0c05476
ACS Omega 2021, 6, 4300−4312

(17) Shafek, S. H.; Abubshait, S. A.; Abubshait, H. A.; Negm, N. A. Antimicrobial potentials and surface activities of novel di-Schiff base nonionic surfactants bearing unsaturated hydrophobic tails. *J. Mol. Liq.* **2019**, *290*, No. 110986.
(18) Verma, C.; Quraishi, M.; Olasunkanmi, L.; Ebenso, E. E. L-Proline-promoted synthesis of 2-amino-4-arylquinoline-3-carbonitriles as sustainable corrosion inhibitors for mild steel in 1 M HCl: experimental and computational studies. *RSC Adv.* **2015**, *5*, 85417−85430.
(19) Saha, S. K.; Dutta, A.; Ghosh, P.; Sukul, D.; Banerjee, P. Adsorption and corrosion inhibition effect of Schiff base molecules on the mild steel surface in 1 M HCl medium: a combined experimental and theoretical approach. *Phys. Chem. Chem. Phys.* **2015**, *17*, 5679−5690.
(20) Saha, S. K.; Murmu, M.; Murmu, N. C.; Banerjee, P. Evaluating electronic structure of quinazolinone and pyrimidinone molecules for its corrosion inhibition effectiveness on target specific mild steel in the acidic medium: a combined DFT and MD simulation study. *J. Mol. Liq.* **2016**, *224*, 629−638.
(21) Ashassi-Sorkhabi, H.; Majidi, M.; Seyyedi, K. Investigation of inhibition effect of some amino acids against steel corrosion in HCl solution. *Appl. Surf. Sci.* **2004**, *225*, 176−185.
(22) Migahed, M. A.; El-Rabiei, M. M.; Nady, H.; Elgendy, A.; Zaki, E. G.; Abdou, M. I.; Noamy, E. S. Novel Ionic Liquid Compound Act as Sweet Corrosion Inhibitors for X-65 Carbon Tubing Steel: Experimental and Theoretical Studies. *J. Bio- Tribo-Corros.* **2017**, *3*, 31.
(23) Singh, A.; Ebenso, E. E.; Quraishi, M.; Lin, Y. 5,10,15,20-Tetra(4-pyridyl)-21H,23H-porphine as an effective corrosion inhibitor for N80 steel in 3.5% NaCl solution. *Int. J. Electrochem. Soc.* **2014**, *9*, 7495−7505.
(24) Shukla, S. K.; Quraishi, M. Cefotaxime sodium: a new and efficient corrosion inhibitor for mild steel in hydrochloric acid solution. *Corros. Sci.* **2009**, *51*, 1007−1011.
(25) El Basiony, N. M.; Elgendy, A.; El-Tabey, A. E.; Al-Sabagh, A. M.; Abd El-Hafez, G. M.; El-raouf, M. A.; Migahed, M. A. Synthesis, characterization, experimental and theoretical calculations (DFT and MC) of ethoxylated aminothiazole as inhibitor for X65 steel corrosion in highly aggressive acidic media. *J. Mol. Liq.* **2020**, *297*, No. 111940.
(26) Mashuga, M. E.; Olasunkanmi, L. O.; Ebenso, E. E. Experimental and theoretical investigation of the inhibitory effect of new pyridazine derivatives for the corrosion of mild steel in 1 M HCl. *J. Mol. Struct.* **2017**, *1136*, 127−139.
(27) ElBelghiti, M.; Karzazi, Y.; Dafali, A.; Hammouti, B.; Bentiss, F.; Obot, I.; Bahadur, I.; Ebenso, E.-E. Experimental, quantum chemical and Monte Carlo simulation studies of 3, 5-disubstituted-4-amino-1, 2, 4-triazoles as corrosion inhibitors on mild steel in acidic medium. *J. Mol. Liq.* **2016**, *218*, 281−293.
(28) McCafferty, E. Validation of corrosion rates measured by the Tafel extrapolation method. *Corros. Sci.* **2005**, *47*, 3202−3215.
(29) Amin, M. A.; El Rehim, S. S. A.; Abdel-Fatah, H. T. Electrochemical frequency modulation and inductively coupled plasma atomic emission spectroscopy methods for monitoring corrosion rates and inhibition of low alloy steel corrosion in HCl solutions and a test for validity of the Tafel extrapolation method. *Corros. Sci.* **2009**, *51*, 882−894.
(30) Shetty, S. D.; Shetty, N.; Parvaz, F.; Agnihotri, K.; Mewawala, P. Investigating the Inhibiting Action of Thiourea Derivative on Mild Steel Corrosion in Acid Medium. *Int. J. Appl. Eng. Res.* **2017**, *12*, 3237−3242.
(31) Atta, N. F.; Fekry, A.; Hassaneen, H. M. Corrosion inhibition, hydrogen evolution and antibacterial properties of newly synthesized organic inhibitors on 316L stainless steel alloy in acid medium. *Int. J. Hydrogen Energy* **2011**, *36*, 6462−6471.
(32) Epelboin, I.; Keddam, M.; Takenouti, H. Use of impedance measurements for the determination of the instant rate of metal corrosion. *J. Appl. Electrochem.* **1972**, *2*, 71−79.
(33) Zhang, G.; Chen, C.; Lu, M.; Chai, C.; Wu, Y. Evaluation of inhibition efficiency of an imidazoline derivative in CO_2-containing aqueous solution. *Mater. Chem. Phys.* **2007**, *105*, 331−340.
(34) Hladky, K.; Callow, L.; Dawson, J. Corrosion rates from impedance measurements: an introduction. *Br. Corros. J.* **1980**, *15*, 20−25.
(35) Abd El-Lateef, H. M. Experimental and computational investigation on the corrosion inhibition characteristics of mild steel by some novel synthesized imines in hydrochloric acid solutions. *Corros. Sci.* **2015**, *92*, 104−117.
(36) Walter, G. A review of impedance plot methods used for corrosion performance analysis of painted metals. *Corros. Sci.* **1986**, *26*, 681−703.
(37) El Basiony, N. M.; Badr, E. E.; Baker, S. A.; El-Tabei, A. S. Experimental and theoretical (DFT&MC) studies for the adsorption of the synthesized Gemini cationic surfactant based on hydrazide moiety as X-65 steel acid corrosion inhibitor. *Appl. Surf. Sci.* **2021**, *539*, No. 148246.
(38) Migahed, M.; Al-Sabagh, A.; Khamis, E.; Zaki, E. Quantum chemical calculations, synthesis and corrosion inhibition efficiency of ethoxylated-[2-(2-{2-[2-(2-benzenesulfonylamino-ethylamino)-ethyl-amino]-ethylamino}-ethylamino)-ethyl]-4-alkyl-benzenesulfonamide on API X65 steel surface under H_2S environment. *J. Mol. Liq.* **2015**, *212*, 360−371.
(39) El Basiony, N. M.; Elgendy, A.; Nady, H.; Migahed, M. A.; Zaki, E. G. Adsorption characteristics and inhibition effect of two Schiff base compounds on corrosion of mild steel in 0.5 M HCl solution: experimental, DFT studies, and Monte Carlo simulation. *RSC Adv.* **2019**, *9*, 10473−10485.
(40) Obot, I.; Obi-Egbedi, N.; Umoren, S. Adsorption characteristics and corrosion inhibitive properties of clotrimazole for aluminium corrosion in hydrochloric acid. *Int. J. Electrochem. Sci.* **2009**, *4*, 863−877.
(41) Sliem, M. H.; El Basiony, N. M.; Zaki, E. G.; Sharaf, M. A.; Abdullah, A. M. Corrosion Inhibition of Mild Steel in Sulfuric Acid by a Newly Synthesized Schiff Base: An Electrochemical, DFT, and Monte Carlo Simulation Study. *Electroanalysis* **2020**, *32*, 3145−3158.
(42) Obot, I.; Obi-Egbedi, N.; Umoren, S. Antifungal drugs as corrosion inhibitors for aluminium in 0.1 M HCl. *Corros. Sci.* **2009**, *51*, 1868−1875.
(43) Quraishi, M.; Ansari, F.; Jamal, D. Thiourea derivatives as corrosion inhibitors for mild steel in formic acid. *Mater. Chem. Phys.* **2003**, *77*, 687−690.
(44) Abd-Elaal, A. A.; Elbasiony, N. M.; Shaban, S. M.; Zaki, E. G. Studying the corrosion inhibition of some prepared nonionic surfactants based on 3-(4-hydroxyphenyl) propanoic acid and estimating the influence of silver nanoparticles on the surface parameters. *J. Mol. Liq.* **2018**, *249*, 304−317.
(45) Al-Sabagh, A. M.; El Basiony, N. M.; Sadeek, S. A.; Migahed, M. A. Scale and corrosion inhibition performance of the newly synthesized anionic surfactant in desalination plants: Experimental, and theoretical investigations. *Desalination* **2018**, *437*, 45−58.
(46) El Nagy, H. A.; El Tamany, E. H.; Ashour, H.; El-Azabawy, O. E.; Zaki, E. G.; Elsaeed, S. M. Polymeric Ionic Liquids Based on Benzimidazole Derivatives as Corrosion Inhibitors for X-65 Carbon Steel Deterioration in Acidic Aqueous Medium: Hydrogen Evolution and Adsorption Studies. *ACS Omega* **2020**, *5*, 30577−30586.
(47) Mobin, M.; Rizvi, M.; Olasunkanmi, L. O.; Ebenso, E. E. Biopolymer from Tragacanth gum as a green corrosion inhibitor for carbon steel in 1 M HCl solution. *ACS Omega* **2017**, *2*, 3997−4008.
(48) Fu, J.; Zang, H.; Wang, Y.; Li, S.; Chen, T.; Liu, X. Experimental and theoretical study on the inhibition performances of quinoxaline and its derivatives for the corrosion of mild steel in hydrochloric acid. *Ind. Eng. Chem. Res.* **2012**, *51*, 6377−6386.
(49) Saha, S. K.; Ghosh, P.; Hens, A.; Murmu, N. C.; Banerjee, P. Density functional theory and molecular dynamics simulation study on corrosion inhibition performance of mild steel by mercapto-quinoline Schiff base corrosion inhibitor. *Physica E* **2015**, *66*, 332−341.
(50) Fouda, A. S.; Ismail, M. A.; Temraz, A. M.; Abousalem, A. S. Comprehensive investigations on the action of cationic terthiophene and bithiophene as corrosion inhibitors: experimental and theoretical studies. *New J. Chem.* **2019**, *43*, 768−789.

https://dx.doi.org/10.1021/acsomega.0c05476
ACS Omega 2021, 6, 4300−4312

(51) Saha, S. K.; Banerjee, P. Introduction of newly synthesized Schiff base molecules as efficient corrosion inhibitors for mild steel in 1 M HCl medium: an experimental, density functional theory and molecular dynamics simulation study. *Mater. Chem. Front.* **2018**, *2*, 1674−1691.
(52) Chen, R.; Fan, F.; Dittrich, T.; Li, C. Imaging photogenerated charge carriers on surfaces and interfaces of photocatalysts with surface photovoltage microscopy. *Chem. Soc. Rev.* **2018**, *47*, 8238−8262.
(53) Guo, L.; Obot, I. B.; Zheng, X.; Shen, X.; Qiang, Y.; Kaya, S.; Kaya, C. Theoretical insight into an empirical rule about organic corrosion inhibitors containing nitrogen, oxygen, and sulfur atoms. *Appl. Surf. Sci.* **2017**, *406*, 301−306.
(54) Masoud, M.; Awad, M.; Shaker, M.; El-Tahawy, M. The role of structural chemistry in the inhibitive performance of some amino-pyrimidines on the corrosion of steel. *Corros. Sci.* **2010**, *52*, 2387−2396.
(55) Mert, B. D.; Yüce, A. O.; Kardaş, G.; Yazıcı, B. Inhibition effect of 2-amino-4-methylpyridine on mild steel corrosion: experimental and theoretical investigation. *Corros. Sci.* **2014**, *85*, 287−295.
(56) Labjar, N.; Bentiss, F.; Lebrini, M.; Jama, C.; El hajjaji, S. Study of Temperature Effect on the Corrosion Inhibition of C38 Carbon Steel Using Amino-tris(Methylenephosphonic) Acid in Hydrochloric Acid Solution. *Int. J. Corros.* **2011**, *2011*, No. 548528.
(57) Al-Sabagh, A.; El Basiony, N.; Sadeek, S.; Migahed, M. Scale and corrosion inhibition performance of the newly synthesized anionic surfactant in desalination plants: experimental, and theoretical investigations. *Desalination* **2018**, *437*, 45−58.
(58) Ebenso, E. E.; Arslan, T.; Kandemirli, F.; Caner, N.; Love, I. Quantum chemical studies of some rhodanine azosulpha drugs as corrosion inhibitors for mild steel in acidic medium. *Int. J. Quantum Chem.* **2010**, *110*, 1003−1018.

NOTE ADDED AFTER ASAP PUBLICATION

Due to a production error, the version of this paper that was published ASAP January 29, 2021, contained a corrupt version of Figure 11. The error was fixed, and the corrected version was posted February 1, 2021.

https://dx.doi.org/10.1021/acsomega.0c05476
ACS Omega 2021, 6, 4300−4312